

## UV and Optical Signatures of Late-time Disk Instabilities in Tidal Disruption Events

DAICHI TSUNA,<sup>1</sup> V. ASHLEY VILLAR,<sup>1,2</sup> ANTHONY L. PIRO,<sup>3</sup> AND SAMANTHA C. WU<sup>3,4</sup>

<sup>1</sup>*Center for Astrophysics | Harvard & Smithsonian, 60 Garden St, Cambridge, MA 02138, USA*

<sup>2</sup>*The NSF AI Institute for Artificial Intelligence and Fundamental Interactions*

<sup>3</sup>*The Observatories of the Carnegie Institution for Science, Pasadena, CA 91101, USA*

<sup>4</sup>*Center for Interdisciplinary Exploration & Research in Astrophysics (CIERA), Physics & Astronomy, Northwestern University, Evanston, IL 60202, USA*

### ABSTRACT

Tidal disruption events (TDEs) are unique probes of evolving accretion in supermassive black holes. Recent models of TDE disks show that they undergo brief thermal instabilities with temporal super-Eddington accretion at late times, which has been suggested as a possibility to explain the ubiquitous late radio emergence in TDEs. We model the ultraviolet (UV) and optical signatures of such disk instabilities, expected from the accretion power being reprocessed by the optically-thick outflow following super-Eddington accretion. Our model predicts brief UV-bright transients lasting for days, with luminosities of  $10^{42}$ – $10^{43}$  erg s<sup>−1</sup> in near-UV and  $10^{41}$ – $10^{42}$  erg s<sup>−1</sup> in optical for a typical TDE by a  $10^6 M_\odot$  black hole. These could be detectable by near-future surveys such as ULTRASAT, Vera C. Rubin Observatory and Argus Array, for TDEs of redshifts out to  $\approx 0.1$ . We further conduct a search for these transients in existing nearby TDEs using data from the Zwicky Transient Facility, placing upper limits on the flare rate for each TDE of 1–2 yr<sup>−1</sup> dependent on the outflow mass. In the era of future surveys, combined UV/optical and radio monitoring would be an important test to the disk instability phenomena, as well as its explanation for the late-time radio emission in TDEs.

### 1. INTRODUCTION

A star is tidally disrupted when it reaches too close to a supermassive black hole (BH), such that tidal forces overwhelm the star’s self-gravity (Hills 1975; Rees 1988; Phinney 1989). These tidal disruption events (TDEs), observed in wavelengths spanning from radio to X-rays, are valuable probes for studying the physics of BH accretion and the environments surrounding supermassive BHs (e.g. Alexander et al. 2020; Gezari 2021; Saxton et al. 2021; Mockler et al. 2025, for reviews).

About half of the disrupted stellar debris is gravitationally bound to the BH and eventually settles to form an accretion disk once its energy and angular momentum are significantly dissipated. The UV plateau observed in a number of TDEs indicates disk formation within a timescale of years after optical peak (van Velzen et al. 2019; Mummery et al. 2024; Guolo et al. 2025).

Meanwhile, radio observations find late time brightening hundreds to thousands of days after optical peak (Horesh et al. 2021; Cendes et al. 2022, 2024; Sfaradi et al. 2024; Golay et al. 2025) for a large fraction of TDEs (40% of optical TDEs; Cendes et al. 2024). Equiparti-

tion analysis of a large sample of TDEs favor the late radio emission in many of them being powered by a delayed launch of mildly relativistic ( $\sim 0.1c$ ) outflows (Cendes et al. 2024; Goodwin et al. 2025). The origin(s) for such delayed outflows is unclear, while recent studies indicate connections with the evolution of the accretion onto the supermassive BH (Alexander et al. 2025).

One possibility to explain the delayed outflow is that the disk formation itself is delayed. Such delayed circularization/disk formation relative to optical peak is argued in recent simulations, while the detailed timescale is still in active debate (e.g., Ryu et al. 2023; Price et al. 2024; Steinberg & Stone 2024; Huang et al. 2024, 2025). Another possibility is thermal instabilities in TDE disks occurring at late times (Lu 2022; Piro & Mockler 2025; Guo & Qiao 2025, but see also Alush & Stone 2025). Under these instabilities the disk can undergo brief, enhanced accretion onto the BH, which often exceeds the Eddington limit and could lead to mildly relativistic outflows (e.g., Jiang & Dai 2024). Recently, Wu et al. (2025) find from detailed radio modeling that the sub-relativistic outflows expected from disk instabilities are a viable possibility to explain many of the events (see also Sato et al. 2025).

As various scenarios of delayed radio emission exist, a key question is whether there could be other unique predictions from such disk instabilities. In this work we consider the emission from the outflow at the onset of such disk accretion flares. We find that the flares are typically accompanied by brief UV-bright transients, lasting for a few days with peak luminosities of  $10^{42}$ – $10^{43}$  erg s $^{-1}$  in near-UV, making this scenario testable in high-cadence UV and optical surveys.

Our work is constructed as follows. In Section 2 we present our model for calculating the UV/optical emission from the accretion flares, and the key features of the light curve evolution. We present a parameter study of this in Section 3, and discuss the prospects of UV/optical surveys to test the existence of disk instabilities using these transients. In Section 4 we present our search for these transients in archival TDEs, using existing high-cadence optical data. We conclude in Section 5.

## 2. EMISSION FROM DISK OUTFLOWS BY THE ACCRETION FLARE

Our model for the accretion flare is inspired by time-dependent one-zone modeling of Piro & Mockler (2025). We have three parameters, the total mass ejected by the accretion flare  $M_{\text{fl}}$ , the flare's duration  $t_{\text{fl}}$ , and the characteristic disk radius  $r_d$  during the flare. Piro & Mockler (2025) find that the flare's duration is nearly independent of both the BH's mass  $M_{\text{BH}}$  and time from disruption, with  $t_{\text{fl}} \approx 1$ – $2$  days. This arises from the disk radius scaling with the tidal radius

$$r_T \approx \left( \frac{M_{\text{BH}}}{M_*} \right)^{1/3} R_* \sim 100 R_\odot \left( \frac{M_{\text{BH}}}{10^6 M_\odot} \right)^{1/3} \left( \frac{M_*}{M_\odot} \right)^{7/15} \quad (1)$$

by a nearly constant factor ( $r_d \sim 5r_T$  in their model at the flaring state), and  $t_{\text{fl}}$  being roughly the viscous time

$$t_{\text{visc}} \approx \frac{1}{\alpha} \sqrt{\frac{r_d^3}{GM_{\text{BH}}}} \sim 2 \text{ day} \left( \frac{r_d}{5r_T} \right)^{3/2} \left( \frac{M_*}{M_\odot} \right)^{7/10}, \quad (2)$$

where  $\alpha \approx 0.1$  is the viscosity parameter. In equation (1) we have used the mass-radius relation of main sequence stars  $R_*/R_\odot \approx (M_*/M_\odot)^{4/5}$ . One sees that the dependence on  $M_{\text{BH}}$  cancels out when  $r_d/r_T$  is fixed.

On the other hand, the value of  $M_{\text{fl}}$  is less certain, as it depends on the accretion history (as well as  $\alpha$  and  $M_{\text{BH}}$ ) which is less clear especially at early times. In this work we take an empirical approach and consider masses of  $M_{\text{fl}} = 10^{-2}$ – $10^{-1} M_\odot$ , motivated by the results of Wu et al. (2025) for explaining both the timescale and luminosity of the delayed radio detections in TDEs.

In this high accretion state, most of the accreted mass is ejected as a wind due to temporal super-Eddington

accretion with rate

$$\dot{M}_w \approx \frac{M_{\text{fl}}}{t_{\text{fl}}} \sim 4 M_\odot \text{ yr}^{-1} \left( \frac{M_{\text{fl}}}{10^{-2} M_\odot} \right) \left( \frac{t_{\text{fl}}}{1 \text{ day}} \right)^{-1}, \quad (3)$$

that highly exceeds the Eddington-limited accretion rate  $\dot{M}_{\text{Edd}} \sim 10^{-2} M_\odot \text{ yr}^{-1} (M_{\text{BH}}/10^6 M_\odot)$ .

We assume the wind is launched quasi-spherically from the disk due to accretion at a characteristic radius  $r_{\text{in}}$  with constant rate  $\dot{M} \approx \dot{M}_w \approx M_{\text{fl}}/t_{\text{fl}}$ , carrying an accretion power of <sup>5</sup>

$$L_{\text{acc}}(t \leq t_{\text{fl}}) \approx \frac{GM_{\text{BH}}\dot{M}_w}{r_{\text{in}}} \sim 2 \times 10^{44} \text{ erg s}^{-1} \left( \frac{\dot{M}_w}{M_\odot \text{ yr}^{-1}} \right) \left( \frac{r_{\text{in}}}{300R_g} \right)^{-1} \quad (4)$$

Here  $R_g = GM_{\text{BH}}/c^2 \sim 1.5 \times 10^{11} \text{ cm} (M_{\text{BH}}/10^6 M_\odot)$  is the BH's gravitational radius. The launching radius  $r_{\text{in}}$  could correspond to the “spherization radius” (Shakura & Sunyaev 1973) inside which the local accretion power exceeds the Eddington limit  $L_{\text{Edd}} = 4\pi GM_{\text{BH}}c/\kappa$ ,

$$r_{\text{Sph}} \approx \frac{\kappa \dot{M}_w}{4\pi c} \sim 5 \times 10^{13} \text{ cm} \left( \frac{\kappa}{0.3 \text{ cm}^2 \text{ g}^{-1}} \right) \left( \frac{\dot{M}_w}{M_\odot \text{ yr}^{-1}} \right), \quad (5)$$

or  $r_{\text{in}} \approx r_d$  if  $r_d < r_{\text{Sph}}$  and the accretion is super-Eddington everywhere in the disk. We therefore adopt

$$r_{\text{in}} = \min(r_d, r_{\text{Sph}}). \quad (6)$$

The opacity  $\kappa$  is expected to be dominated by scattering opacity for the density and temperature of our interest, and we adopt a constant  $\kappa \approx 0.3 \text{ cm}^2 \text{ g}^{-1}$  for a solar-like composition.

At  $r_{\text{in}}$  we expect the accretion power to be shared nearly equally by internal and kinetic energy, but the wind is highly optically thick. Due to adiabatic expansion, internal energy is degraded as it is converted to kinetic energy via PdV work, and the observed luminosity is generally reduced from  $L_{\text{acc}}$ .

Our aim is to semi-analytically calculate the emission from such time-dependent wind outflows. We follow the spirit of Piro & Lu (2020) (see their Figure 1 for context), but we build the model slightly differently so that it can properly solve under abrupt changes in the accretion power and outflow like considered here.

<sup>5</sup> For our expected case of  $r_{\text{in}} \sim 10^2$ – $10^3 R_g$ , this formulation results in an energy efficiency  $L_{\text{acc}}/\dot{M}_w c^2$  roughly consistent with the efficiency of  $\sim 0.1$ – $1$  % obtained in numerical simulations of super-Eddington disks (e.g., Jiang et al. 2019; Yoshioka et al. 2024; Zhang et al. 2025).

### 2.1. Light curve

Our approach below is to split the wind into multiple “shells” launched at times  $\tilde{t}$  ( $0 < \tilde{t} < t_{\text{fl}}$ ) and calculate the radiative output of each shell at time  $t'$  from launch, to obtain the luminosity observed at time  $t = \tilde{t} + t'$ .

Let us consider a shell of wind material launched over a time  $\Delta t$  at radius  $r_{\text{in}}$  and time  $\tilde{t}$ , with internal energy

$$E_{\text{int},0} \approx \frac{1}{2} L_{\text{acc}} \Delta t \quad (7)$$

and with velocity

$$v_w \sim \sqrt{(L_{\text{acc}}/2)/(\dot{M}_w/2)} \sim 0.06c \left( \frac{r_{\text{in}}}{300R_g} \right)^{-1/2}. \quad (8)$$

At a time  $t'$  from launch, the shell increases its volume as  $V_{\text{sh}} = 4\pi[r_{\text{in}} + (v_w t')]^2(v_w \Delta t)$ , and its internal energy  $E_{\text{int}}$  (assumed to be radiation dominated) evolves as

$$\begin{aligned} \frac{dE_{\text{int}}}{dt'} &= -\frac{E_{\text{int}}}{3V_{\text{sh}}} \frac{dV_{\text{sh}}}{dt'} - L_{\text{rad}} \\ &= -\frac{2E_{\text{int}}}{3(t' + r_{\text{in}}/v_w)} - \frac{E_{\text{int}}}{t_{\text{diff}}}, \end{aligned} \quad (9)$$

where the first term is adiabatic cooling by PdV work, and the second term is the radiative cooling regulated by the diffusion of photons through the wind over a timescale (Piro & Lu 2020)

$$\begin{aligned} t_{\text{diff}} &\approx \frac{\kappa \dot{M}_w}{4\pi v_w c} \times \left[ \frac{r_w - (r_{\text{in}} + v_w t')}{r_w} \right]^2 \\ &\approx \frac{\kappa \dot{M}_w}{4\pi v_w c} \times \left[ \frac{v_w \tilde{t}}{r_{\text{in}} + v_w(\tilde{t} + t')} \right]^2 \end{aligned} \quad (10)$$

Here  $r_w = r_{\text{in}} + v_w(\tilde{t} + t')$  is the outer edge of the wind. The differential equation in  $t'$  has an analytical solution, with initial condition of  $E_{\text{int}} = E_{\text{int},0}$  at  $t' = 0$ , of

$$\begin{aligned} E_{\text{int}}(t') &= E_{\text{int},0} \left( \frac{r_{\text{in}}}{r_{\text{in}} + v_w t'} \right)^{2/3} \\ &\times \exp \left\{ -\frac{B^3}{3A} \left[ \left( 1 + \frac{1}{B} \frac{t'}{\tilde{t}} \right)^3 - 1 \right] \right\} \end{aligned} \quad (11)$$

where  $A, B$  are dimensionless parameters that are independent of  $t'$ ,

$$A = \frac{1}{\tilde{t}} \frac{\kappa \dot{M}_w}{4\pi v_w c}, \quad B = 1 + \frac{r_{\text{in}}}{v_w \tilde{t}}. \quad (12)$$

The corresponding luminosity  $L_{\text{rad}} = E_{\text{int}}/t_{\text{diff}}$  is

$$\begin{aligned} L_{\text{rad}}(t') &= \frac{L_{\text{acc}} \Delta t}{2A\tilde{t}} \left( B + \frac{t'}{\tilde{t}} \right)^2 \left( \frac{r_{\text{in}}}{r_{\text{in}} + v_w t'} \right)^{2/3} \\ &\times \exp \left\{ -\frac{B^3}{3A} \left[ \left( 1 + \frac{1}{B} \frac{t'}{\tilde{t}} \right)^3 - 1 \right] \right\}. \end{aligned} \quad (13)$$

We can now integrate over all the emitted shells to obtain the light curve as a function of  $t$ . Using the solution for  $L_{\text{rad}}(t')$  and substituting  $t' = t - \tilde{t}$  for each wind shell launched at  $\tilde{t}$ , we sum up the contributions from all shells emitted within  $t$  and obtain

$$\begin{aligned} L_{\text{obs}}(t) &= \int_0^t d\tilde{t} \frac{L_{\text{acc}}(\tilde{t})}{2A\tilde{t}} \left( B + \frac{t - \tilde{t}}{\tilde{t}} \right)^2 \left[ \frac{r_{\text{in}}}{r_{\text{in}} + v_w(t - \tilde{t})} \right]^{2/3} \\ &\times \exp \left\{ -\frac{B^3}{3A} \left[ \left( 1 + \frac{1}{B} \frac{t - \tilde{t}}{\tilde{t}} \right)^3 - 1 \right] \right\}, \end{aligned} \quad (14)$$

The top-left panel of Figure 1 shows a light curve for our fiducial parameter set of  $M_{\text{BH}} = 10^6 M_{\odot}$ ,  $M_{\text{fl}} = 0.02 M_{\odot}$ ,  $r_d = 300R_g$ , and  $t_{\text{fl}} = 2$  days. After a brief decline during  $t \ll r_{\text{in}}/v_w \sim 0.3$  days as the diffusion time evolves (Piro & Lu 2020), the light curve settles to a plateau-like morphology. The plateau is partly due to our assumed top-hat time-dependence of  $\dot{M}$  and  $L_{\text{acc}}$ . The observed luminosity at this phase is a factor of several lower than the input luminosity  $L_{\text{acc}}$  due to the adiabatic loss. Once the outflow shuts off at  $t = t_{\text{fl}}$ , the light curve drops sharply over a timescale of a few days, which is set by the diffusion timescale in the wind.

### 2.2. Temperature Evolution

We calculate the temperature of the emission by approximately solving the reprocessing by the wind. Following Piro & Lu (2020), we obtain this by calculating the color radius  $r_c$ , the outermost radius where thermalization occurs.

At a given time  $t$ , the density profile of the wind varies during and after the flare as

$$\rho(r, t < t_{\text{fl}}) = \frac{\dot{M}_w}{4\pi r^2 v_w} \quad (r < r_w = r_{\text{in}} + v_w t), \quad (15)$$

$$\rho(r, t > t_{\text{fl}}) = \begin{cases} \frac{\dot{M}_w}{4\pi r^2 v_w} & (r_{\text{in}} + v_w(t - t_{\text{fl}}) < r < r_w) \\ 0 & (\text{otherwise}). \end{cases} \quad (16)$$

The diffusion time in equation (10) indicates that the bulk of the radiation is emitted around while the wind expands out to the trapping radius

$$r_{\text{tr}} \approx r_{\text{in}} + \frac{\kappa \dot{M}_w}{4\pi c}. \quad (17)$$

At the earliest stage when  $r_w < r_{\text{tr}}$ , photons travel by advection throughout the wind, and we adopt the temperature set by adiabatic cooling out to the outermost radius of the wind, with  $r_c \approx r_w$  and

$$T_{\text{obs}} \approx \left( \frac{L_{\text{obs}}}{4\pi r_w^2 v_w a} \right)^{1/4}. \quad (18)$$

Once  $r_w > r_{\text{tr}}$ , above  $r_{\text{tr}}$  the luminosity is roughly constant, and the temperature could be well-represented by

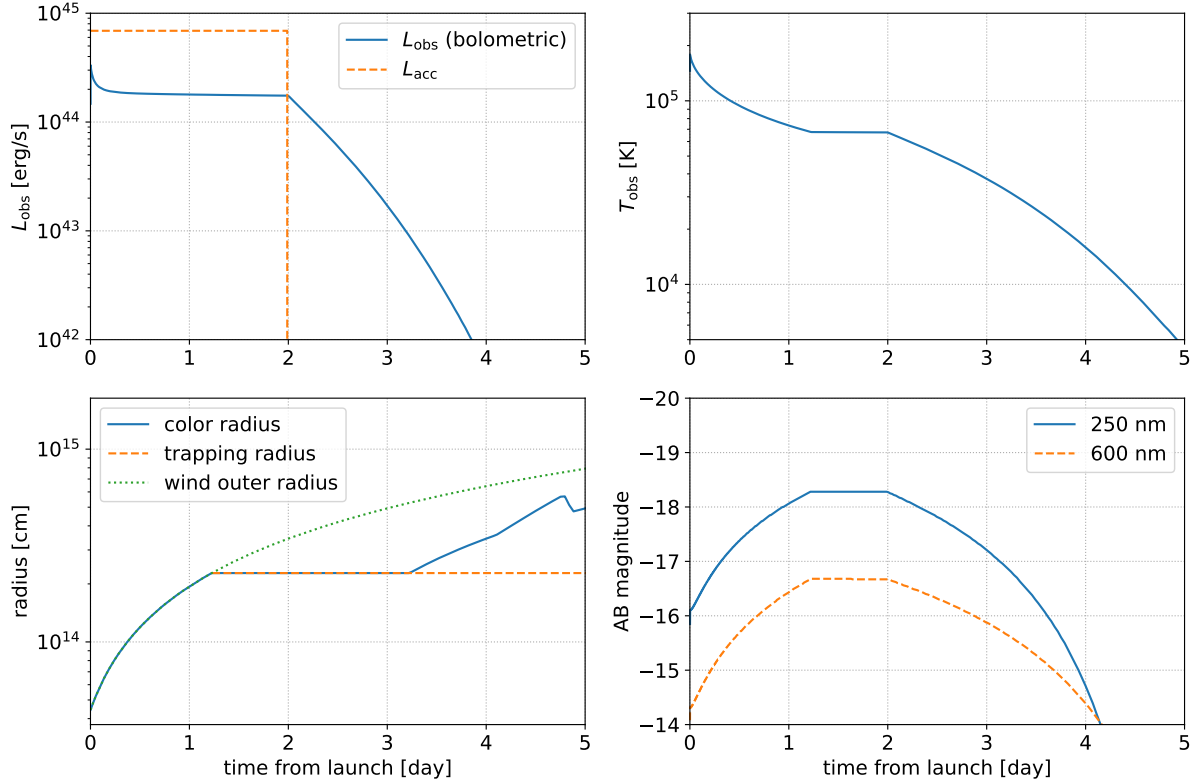


**Figure 1.** Light curve predictions for parameters:  $M_{\text{BH}} = 10^6 M_{\odot}$ ,  $r_d = 300 R_g$ ,  $M_{\text{fl}} = 0.02 M_{\odot}$ , and  $t_{\text{fl}} = 2$  days. Top panels show the bolometric luminosity and emission temperature, and the bottom right panel shows the AB magnitudes in the near-UV and optical under a greybody approximation. Bottom left panel shows the evolution of various radii defined in Section 2.2.

the diffusion approximation as (Piro & Lu 2020)

$$L_{\text{obs}} = -\frac{4\pi r^2 ac}{3\kappa\rho} \frac{\partial T^4}{\partial r}. \quad (19)$$

This leads to a temperature profile

$$T(r, t)^4 \approx T_{\text{out}}^4 + \int_r^{r_w} \frac{3\kappa\rho L_{\text{obs}}}{4\pi r^2 ac}, \quad (20)$$

where  $T_{\text{out}}$  is the temperature at the outer edge, which we solve for by fixing the temperature at  $r_{\text{tr}}$  as

$$T(r = r_{\text{tr}}, t) \approx \left( \frac{L_{\text{obs}}}{4\pi r_{\text{tr}}^2 v_w a} \right)^{1/4}. \quad (21)$$

In the density regimes of interest the opacity is scattering-dominated, and the color radius  $r_c(t)$  that determines the temperature is interior to the photosphere. This radius is solved by

$$\int_{r_c}^{r_w} \sqrt{3\kappa_{\text{abs}}\kappa} \rho dr = 1 \quad (22)$$

For  $\kappa_{\text{abs}}$ , we adopt a Kramer's opacity law motivated for bound-free and free-free absorption, with a sharp cutoff at low temperatures due to hydrogen recombination

$$\kappa_{\text{abs}}(\rho, T) = \begin{cases} C\rho T^{-3.5} & (T \geq T_{\text{rec}}) \\ C\rho T_{\text{rec}}^{-3.5} (T/T_{\text{rec}})^{\beta} & (T < T_{\text{rec}}), \end{cases} \quad (23)$$

where the parameters are in cgs units, and  $C$ ,  $T_{\text{rec}}$  are dependent on the composition of the wind. Here we set  $\beta = 15$  to mimic the sharp cutoff at  $T < T_{\text{rec}}$ , and adopt constant values  $(C, T_{\text{rec}}) = (4 \times 10^{25} \text{ cgs}, 6000 \text{ K})$  motivated for solar abundance gas (e.g. Appendix of Matsumoto & Piran 2021). The detailed choice of  $\beta$  does not affect our conclusions, as we later find emission temperatures to be much larger than  $T_{\text{rec}}$ .

When  $r_c$  solved by this procedure satisfies  $r_c > r_{\text{tr}}$  (“thermalization-dominated temperature” in Piro & Lu 2020),  $T_{\text{obs}}$  would be the temperature at the color radius

$$T_{\text{obs}} \approx \left[ T_{\text{out}}^4 + \int_{r_c}^{r_w} \frac{3\kappa\rho L_{\text{obs}}}{4\pi r^2 ac} \right]^{1/4} (r_c > r_{\text{tr}}). \quad (24)$$

On the other hand if  $r_c < r_{\text{tr}}$  (“trapping-dominated temperature” in Piro & Lu 2020), the temperature of the emission is set by the trapping radius. We adopt the temperature at  $r_{\text{tr}}$  of

$$T_{\text{obs}} \approx \left( \frac{L_{\text{obs}}}{4\pi r_{\text{tr}}^2 v_w a} \right)^{1/4} (r_c < r_{\text{tr}}), \quad (25)$$

and update  $r_c = r_{\text{tr}}$ .

The temperature predictions solved this way is shown in the top-right panel of Figure 1. Initially photons

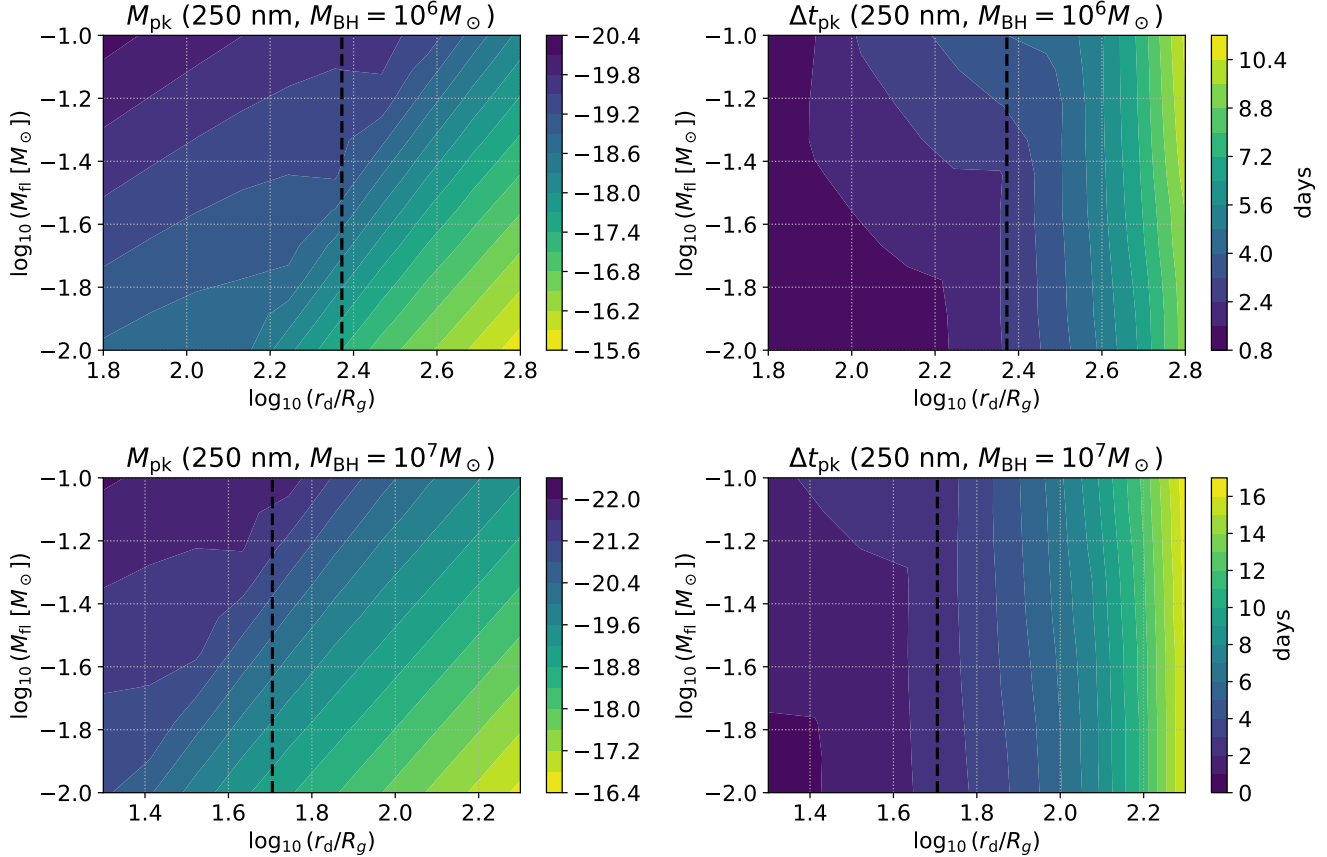


**Figure 2.** Emission properties in the near-UV (250 nm). Left and right panels respectively show the peak magnitude and duration within 1 mag from peak. Top and bottom panels are respectively for  $M_{\text{BH}} = 10^6, 10^7 M_{\odot}$ . Vertical dashed lines show the radius  $r_d \approx 5r_T$  inspired from the model of Piro & Mockler (2025), where  $r_T$  is the tidal radius (see main text).

are completely advected by the wind, and the temperature drops as given in equation (18). Then it enters the trapping-dominated temperature where  $T_{\text{obs}}$  is set by equation (25). Here  $T_{\text{obs}}$  plateaus at  $\approx 1\text{--}2$  days because both  $L_{\text{obs}}$  and  $r_{\text{tr}}$  are nearly constants. The plateau only appears at sufficiently low values of  $M_{\text{fl}}$  when  $r_{\text{tr}}/v_w < t_{\text{fl}}$  is satisfied. For much larger  $M_{\text{fl}}$  (and  $r_{\text{tr}}$ ), the trapping-dominated regime enters only at  $t > t_{\text{fl}}$ , and  $T_{\text{obs}}$  would then monotonically decline with time because  $L_{\text{obs}}(t > t_{\text{fl}})$  drops with time.

Since  $\kappa_{\text{obs}}$  is strongly temperature-dependent as  $\kappa_{\text{abs}} \propto T^{-3.5}$ , the thermalization-dominated regime (where  $r_c > r_{\text{tr}}$ ) enters only when the temperature at the outer edge of the wind becomes low enough, about  $10^4$  K for this parameter set. The kink in the color radius evolution after this reflects the strong turnover of  $\kappa_{\text{abs}}$  around  $T = T_{\text{rec}}$ .

In the bottom-right panel of Figure 1 we show predictions for the AB magnitude in the near-UV (250 nm) and optical (600 nm), assuming the transient has greybody spectra with temperature  $T_{\text{obs}}$  and luminosity  $L_{\text{obs}}$ . Due

to the high temperature of  $\sim 10^5$  K at early times, the AB magnitudes peak closer to the end of the flare. For this fiducial case, the magnitudes in near-UV (optical) are  $< -17$  mag ( $< -15$  mag) over a few days. The top-hat feature of the light curve in these bands is again due to our adopted time-dependence for  $\dot{M}$  and  $L_{\text{acc}}$ , and could more smoothly evolve in reality.

### 3. PARAMETER EXPLORATION

The most promising instruments to detect these transients are surveys with short cadences around a few days or less, such as the Zwicky Transient Facility (ZTF; Bellm et al. 2019), ULTRASAT (Shvartzvald et al. 2024) and Vera C. Rubin Observatory’s Legacy Survey of Space and Time (LSST; Ivezić et al. 2019). The detectability of these flares in optical and UV vary by both  $r_d$  and  $M_{\text{fl}}$ , as they control both the energetics and temperature of the flare. We calculate a grid of light curves varying these two parameters, and measure the peak magnitudes  $M_{\text{pk}}$  and duration  $\Delta t_{\text{pk}}$  of the light curve within 1 mag from peak.

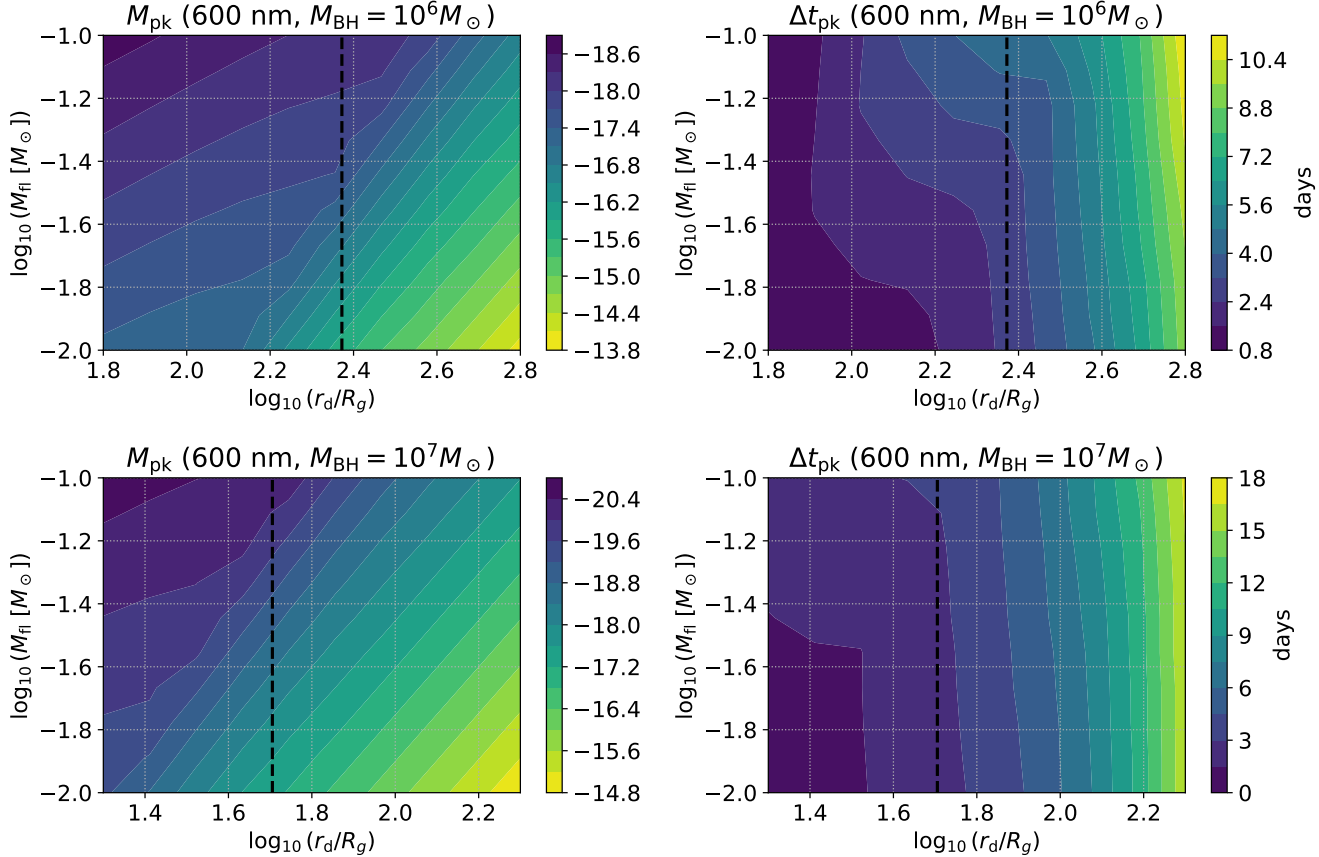


**Figure 3.** Same as Figure 3, but for the optical (600 nm).

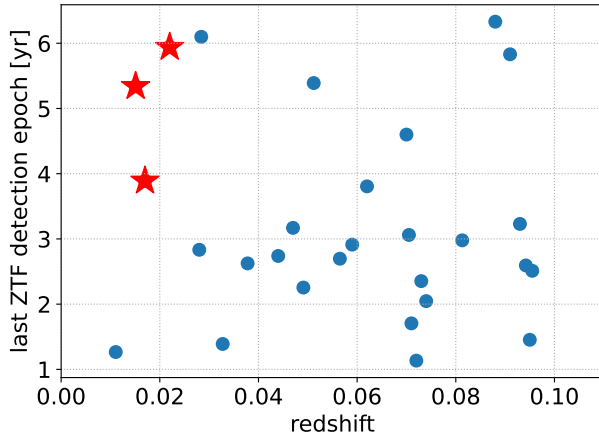
We adopt  $M_{\text{fl}} = 0.01\text{--}0.1 M_{\odot}$  favored from late time radio emission modeling (Wu et al. 2025), and choose a range of  $r_d$  around  $r_d \approx 5r_T$  approximately found in the model of Piro & Mockler (2025). This value of  $r_d$ , corresponding to the disk's outer radius, is also roughly reproduced in multi-wavelength analyses of late-time plateau emission in TDEs (Guolo et al. 2025, their Figure 7). We set the flare duration  $t_{\text{fl}}$  as the viscous time of the disk, scaling with  $r_d$  as in equation 2 (with  $M_* = M_{\odot}$ ).

Figure 2 shows the range of  $M_{\text{pk}}$  and  $\Delta t_{\text{pk}}$  at near-UV (250 nm) for the parameter space of  $r_d$  and  $M_{\text{fl}}$ , with  $M_{\text{BH}}$  of  $10^6 M_{\odot}$  and  $10^7 M_{\odot}$  in the top and bottom panels. For our fiducial choice of  $r_d = 5r_T$  (dashed lines) and  $M_{\text{BH}} = 10^6 M_{\odot}$ , we find the near-UV emission to peak at magnitudes between  $-17$  and  $-19$  mag, with durations of 3–4 days. ULTRASAT, with a single-visit sensitivity of 22.5 mag at 250 nm and a cadence of 4 days (Shvartzvald et al. 2024), could detect such late-time UV flares in a large fraction of TDEs out to redshift  $z \approx 0.1$ . Thus combined UV and radio monitoring would offer strong direct tests for the disk instability scenario, as radio measurements can infer (under the equipartition assumption) the radius evolution and

hence the launch time of the super-Eddington outflow. The case of a  $10^7 M_{\odot}$  BH predicts brighter flares for the same assumptions of  $r_d = 5r_T$ , as the launch radius scaled by the BH's gravitational radius  $r_{\text{in}}/r_g$  is smaller (equation 4). However, this also leads to a faster wind velocity and hence a shorter duration ( $\lesssim 3$  days).

Figure 3 shows the same parameter grid as Figure 2 but for the optical at 600 nm. For a typical SMBH mass of  $M_{\text{BH}} = 10^6 M_{\odot}$  and  $r_d \approx 5r_T$ , the emission in the optical is  $\approx (-14)\text{--}(-17)$  mag ( $10^{41}\text{--}10^{42}$  erg s $^{-1}$ ) and lasts for 3–5 days. This emission would be buried by the main TDE emission at early times but may be visible on year timescales after the optical peak. Such emission would be good targets in the Rubin era, for sources also out to  $z \approx 0.1$ .

A confident detection of the flare may require detection over multiple epochs, which is generally challenging for the predicted short durations of the flares. The Argus Array (Law et al. 2022), with deep co-added sensitivity for  $\approx 23$  mag for a day cadence, would be particularly powerful for this purpose. The LSST deep drilling field could also be similarly powerful (Gris et al. 2023), for a small subset of TDEs that occur in the field.



**Figure 4.** Redshift and epoch of last ZTF detection (relative to discovery), for the 28 TDE samples analyzed in this work. Stars show three TDEs used for constraints on the flare rate, AT 2019qiz, AT 2019azh, and AT 2021ehb (see main text).

#### 4. SEARCH IN OPTICAL LIGHT CURVE DATA OF EXISTING TIDAL DISRUPTION EVENTS

Given the flare’s luminosity, we expect that the flares may even be detectable by existing optical surveys, especially for nearby TDEs that result in brighter flares. For example, TDEs at distances  $\lesssim 100$  Mpc could have flares of  $\lesssim 21$  mag in optical, potentially within reach of surveys like ZTF.

Motivated by this, we conduct a search of late-time flares in existing TDEs, using light curve data from the OTTER database (Franz et al. 2025). We select a sample of 28 TDEs with (i) redshift less than 0.1, (ii) host correction applied, and (iii) with at least one ZTF detection (flagged by  $> 3\sigma$  confidence in OTTER) at  $> 1$  year from discovery. We show the redshift and the epoch of the last ZTF detection (from discovery) in Figure 4 (for details of the events see Appendix A). About half of the samples have detections as late as 3 years after discovery, and four TDEs are at luminosity distances  $D_L < 100$  Mpc.

As TDEs generally have disk-dominated plateau emission at late times (e.g., van Velzen et al. 2019), we search for any short-duration excess that could be consistent with a flare on top of a longer plateau. For each TDE, we extract all host-subtracted ZTF data at  $> 1$  yr from discovery, and compare the flux of each detection with the surrounding flux measurements in the same band at  $\pm(3\text{--}50)$  days. Assuming the flux uncertainties are Gaussian, we estimate the significance as  $\min[(F - f)/\sqrt{dF^2 + df^2}]$ , evaluated using all the surrounding flux measurements  $f \pm df$  around the detection with flux  $F \pm dF$ . We exclude measurements within 3

days as they could be part of a single flare, and beyond 50 days to prevent multiple flares from blending into the analysis. Our search is hence less sensitive to flares frequently occurring with intervals  $\lesssim 50$  days, as the flares can blend into both  $F$  and  $f$ . However we believe these short intervals are unlikely at  $\gtrsim 1$  yr after the TDE, based on existing disk models (Lu 2022; Piro & Mockler 2025).

Our analysis did not find any strong candidates of a disk instability flare. The excess found with high significance were all second peaks of events claimed as repeating (partial) TDEs in the literature, AT 2020vdq (Somalwar et al. 2025a) and AT 2022dbl (Lin et al. 2024; Hinkle et al. 2024). These have luminous peaks ( $\nu L_\nu \sim 10^{43}$  erg s $^{-1}$ ) and slow declines ( $\approx 1$  month) in the optical, inconsistent with the expectations from our model in Section 3. Hence we believe these excesses are unlikely to be due to disk instabilities.

The remaining candidates are all low significance and not strong enough to claim a detection. In Figure 5 we show the two highest-significance candidates from AT2021nwa and AT2019azh, which are both flagged as an  $r$ -band excess. We believe these candidates are also unlikely to be disk instability flares, as the  $g$ -band flux in the vicinity of each candidate is not enhanced like the  $r$ -band flux.

We finally place rough rate constraints of these flares by artificial injections of our theoretical light curve models into ZTF data. For this purpose we focus our analysis on the three most constraining TDEs, which are nearby ( $D_L < 100$  Mpc) and have long ZTF baselines of several years: AT 2019qiz, AT 2019azh, and AT 2021ehb.

Into the observed data, we add signals of flux

$$f_\nu = \frac{1+z}{4\pi D_L^2} L_{\nu'} [L_{\text{obs}}, T_{\text{obs}}], \quad (26)$$

where  $\nu' = (1+z)\nu$  is the source-frame frequency and  $L_{\nu'}$  is calculated assuming a blackbody (at source-frame) with bolometric luminosity  $L_{\text{obs}}$  and temperature  $T_{\text{obs}}$ . The observer-frame frequency  $\nu$  is represented with the central frequency of each filter,  $6.34 \times 10^{14}$  Hz and  $4.72 \times 10^{14}$  Hz for  $g$  and  $r$  band respectively. For the signal we again vary the flare mass as  $M_{\text{fl}} = 0.01\text{--}0.1 M_\odot$ , while we fix the disk radius as  $r_d = 5r_T$  and adopt (median) supermassive BH masses inferred from host galaxy scaling relations (Yao et al. 2023, see Table 1 for their values).

The injections are done from 1 year after discovery to the last ZTF observation sampled by 0.1 day interval, and the same search is repeated for each injection made. By requiring each signal model to not be recovered by the search with  $> 5\sigma$  significance in all ZTF

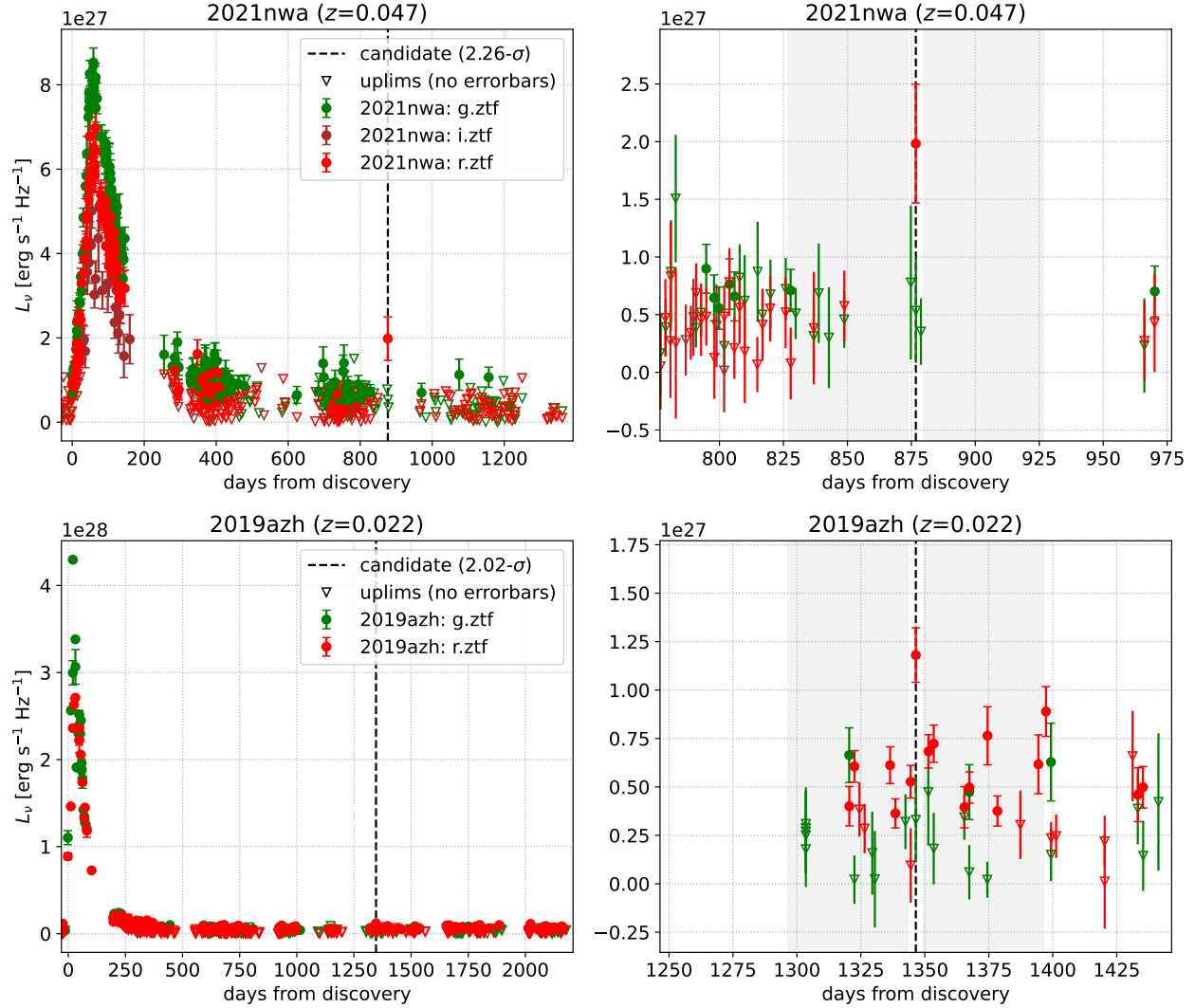


**Figure 5.** The two highest-significance candidates found in our analysis, from AT2019azh and AT2021nwa. Left panels show the full light curve, while the right panels show that at  $\pm 100$  days around the candidate. Shaded regions show the temporal regions used in our search for the flux comparison.

bands, we set the constraint on the rate of the signal. We assume the flares occur according to a Poisson process, a model-agnostic simplification which could be potentially improved in future works by employing detailed model predictions of the flare pattern.

Figure 6 shows the 90% confidence upper limit on the event rate as a function of the flare mass  $M_{\text{fl}}$ . We overall find a constraint of  $\lesssim 1\text{--}2 \text{ yr}^{-1}$  for each of the three TDEs, stronger for higher  $M_{\text{fl}}$ . For the two closer TDEs AT 2019qiz (65 Mpc) and 2021ehb (73 Mpc), the dependence on  $M_{\text{fl}}$  is rather weak. For the furthest AT 2019azh (95 Mpc) the dependence on  $M_{\text{fl}}$  becomes stronger at low  $M_{\text{fl}}$  due to limitation in sensitivity.

At 1–5 years from TDE, the disk instability model of Piro & Mockler (2025) predicts flares occurring about 1 – (a few) times, with higher rates for lower  $M_{\text{BH}}$  and

higher viscosity parameter  $\alpha$ . Our constraints of  $\lesssim 1\text{--}2 \text{ yr}^{-1}$  therefore does not immediately rule out this model, but is quite marginal. We expect the search to be more sensitive in the future, with longer baselines and higher sensitivities to be realized for more TDEs.

## 5. CONCLUSION

We have studied the transient UV and optical emission from accretion disks formed in TDEs, under the picture suggested from recent models that they undergo late-time thermal instabilities. Such instabilities may also explain the emergence of late-time radio emission, seen in a significant fraction of TDEs (e.g., Wu et al. 2025).

We find that the emission from such disk instabilities is expected to be a very hot (a few –  $10 \times 10^4$  K), luminous transient with luminosities of  $10^{42}\text{--}10^{43}$  erg s $^{-1}$

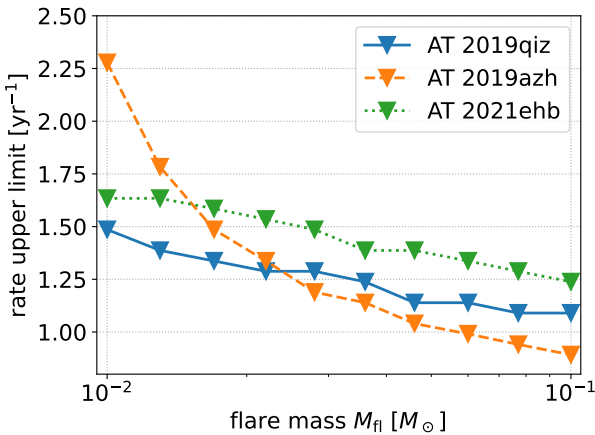


**Figure 6.** 90% confidence upper limits on the flare event rate as a function of flare mass  $M_{\text{fl}}$ , for the three TDEs, AT 2019qiz, AT 2019azh, and AT 2021ehb.

in the near-UV. The near-UV magnitude peaks between  $-17$  and  $-19$  mag, which is a promising target for ULTRASAT for TDEs out to redshift  $\approx 0.1$ . The optical emission is expected to be an order of magnitude fainter, but may still be well constraining in the era of future high-cadence surveys like LSST and Argus Array.

We finally conducted a search for these transient flares in the sample of 28 nearby TDEs (redshift  $< 0.1$ ) using optical data from ZTF. We did not find any promising candidates from late-time photometric detections. The non-detection led to upper limits in their event rates of  $1\text{--}2 \text{ yr}^{-1}$ , for each of the three most constraining TDEs.

We conclude with suggestions for potential improvements to theoretical predictions and observational searches. First, the disk modeling could be improved by extending the one-zone model (e.g., Lu 2022; Piro &

Mockler 2025) to a more realistic 1D/2D model, and/or including the effects of delayed circularization over a timescale of months to years as suggested in recent numerical studies. This could provide more robust predictions for both the timing and the mass of the flares. Second, the greybody assumption for the spectra could be improved by detailed radiative transfer modeling of the outflow, which could impact more on the predictions for optical that are far from the spectral peak. Finally the search can be improved in several ways as more sensitive surveys are realized, such as combining information of multiple filters and applying more physically informed priors on the flares for significance estimates and rate constraints.

## ACKNOWLEDGMENTS

We thank Kate Alexander and Noah Franz for discussions on OTTER data, Xiaoshan Huang, Brenna Mockler, David Sand and members of Edo Berger’s group for discussions, and Assaf Horesh for comments that motivated this study. D. T. is supported by Harvard University through the Institute for Theory and Computation Fellowship. The Villar Astro Time Lab acknowledges support through the David and Lucile Packard Foundation, the Research Corporation for Scientific Advancement (through a Cottrell Fellowship), the National Science Foundation under AST-2433718, AST-2407922 and AST-2406110, as well as an Aramont Fellowship for Emerging Science Research. This work is supported by the National Science Foundation under Cooperative Agreement PHY-2019786 (the NSF AI Institute for Artificial Intelligence and Fundamental Interactions).

## APPENDIX

### A. TDE SAMPLE

We summarize our sample of 28 low-redshift TDEs analyzed in this work (Section 4). The information for these TDEs and their host-subtracted photometric data were obtained from the literature, via the OTTER database<sup>6</sup> (Franz et al. 2025) as of December 2025.

Table 1 shows the redshift, last ZTF detection from discovery, published mass estimates of the supermassive BH, and references for the photometric data and the quoted BH mass. Figure 7 shows the ZTF light curves

of each event, comparing with the expected flare magnitude discussed in Section 3.

<sup>6</sup> <https://otter.idies.jhu.edu>

**Table 1.** Redshift ( $z$ ), luminosity distance ( $D_L$ ), epoch of last ZTF detection from discovery, and the supermassive BH mass estimates (obtained by host galaxy scaling relation, or light curve modeling if not available), for the 28 TDEs analyzed in this work.  $D_L$  is calculated assuming a flat  $\Lambda$ CDM cosmology with parameters  $H_0 = 70 \text{ km s}^{-1} \text{ Mpc}^{-1}$ ,  $\Omega_m = 0.3$  and  $\Omega_\Lambda = 0.7$ .

Event	$z$ ( $D_L$ [Mpc])	Last detection [yr]	$\log_{10}(M_{\text{BH}}[M_\odot])$	References
2018hco	0.0880 (401)	6.33	$6.5 \pm 0.3$	a, b, c
2018lna	0.0910 (416)	5.83	$5.2 \pm 0.4$	a, b, d
2019azh	0.0220 (95)	5.94	$6.4 \pm 0.3$	a, b, d, e, f, g
2019dsg	0.0512 (227)	5.39	$6.9 \pm 0.3$	a, b, d
2019ehz	0.0740 (334)	2.05	$5.7 \pm 0.6$	a, b, d
2019eve	0.0813 (369)	2.98	$5.1 \pm 0.4$	a, b, d
2019qiz	0.0151 (65)	5.34	$6.5 \pm 0.3$	a, b, d, h
2020ksf	0.0942 (431)	2.59	$6.1 \pm 0.4$	b, i
2020mbq	0.0930 (426)	3.23	$\approx 6.08$	b, j
2020mot	0.0700 (315)	4.60	$6.7 \pm 0.3$	b, d, j
2020neh	0.0620 (278)	3.81	$5.4 \pm 0.5$	b, d, k
2020ocn	0.0705 (318)	3.06	$6.4 \pm 0.6$	b, j, l
2020vdq	0.0440 (194)	2.74	$5.6 \pm 0.4$	b, d, m
2020zso	0.0565 (252)	2.70	$6.2 \pm 0.3$	b, j, n
2021ehb	0.0170 (73)	3.89	$7.2 \pm 0.3$	b, d, o
2021mhg	0.0730 (329)	2.35	$6.1 \pm 0.4$	b, d
2021nwa	0.0470 (208)	3.17	$7.2 \pm 0.3$	b, d, p
2021sdu	0.0590 (264)	2.91	$6.7 \pm 0.3$	b, d
2022bdw	0.0378 (166)	2.62	$6.2 \pm 0.5$	b, p
2022dbl	0.0284 (124)	6.10	$6.4 \pm 0.3$	b, q
2022dyt	0.0720 (325)	1.13	$6.3 \pm 0.3$	b, r
2022exr	0.0955 (438)	2.51	$5.4 \pm 0.3$	b, r
2022gri	0.0280 (122)	2.83	$6.2 \pm 0.3$	b, s
2022lri	0.0328 (143)	1.39	$5.0 \pm 0.5$	b, t
2022pna	0.0950 (435)	1.45	$6.7 \pm 0.4$	b, r
2022wtn	0.0491 (218)	2.25	$\approx 6.1$	b, u
2023clx	0.0111 (47)	1.27	$\approx 6$	b, v
2023cvb	0.0710 (320)	1.71	$7.5 \pm 0.2$	b, r

**References**—a: [van Velzen et al. \(2021\)](#), b: [Mummery et al. \(2024\)](#), c: [Alexander et al. \(2025\)](#), d: [Yao et al. \(2023\)](#), e: [Hinkle et al. \(2021\)](#), f: [Liu et al. \(2022\)](#), g: [Faris et al. \(2024\)](#), h: [Nicholl et al. \(2020\)](#), i: [Wevers et al. \(2024\)](#), j: [Hammerstein et al. \(2023\)](#), k: [Angus et al. \(2022\)](#), l: [Pasham et al. \(2024\)](#), m: [Somalwar et al. \(2025b\)](#), n: [Wevers et al. \(2022\)](#), o: [Yao et al. \(2022\)](#), p: [Mummery & van Velzen \(2025\)](#), q: [Lin et al. \(2024\)](#), r: [Mummery \(2026\)](#), s: [Zhu et al. \(2025\)](#), t: [Yao et al. \(2024\)](#), u: [Onori et al. \(2025\)](#), v: [Charalampopoulos et al. \(2024\)](#)

NOTE—For AT 2022dbl there is an observation in 2018 labeled as “detection” by OTTER, which could be an image subtraction artifact ([Makrygianni et al. 2025](#)). While we include this as discovery, whether including this as detection or not does not influence our conclusions.

## REFERENCES

Alexander, K. D., van Velzen, S., Horesh, A., & Zauderer, B. A. 2020, SSRv, 216, 81, doi: [10.1007/s11214-020-00702-w](https://doi.org/10.1007/s11214-020-00702-w)

Alexander, K. D., Margutti, R., Gomez, S., et al. 2025, arXiv e-prints, arXiv:2506.12729, doi: [10.48550/arXiv.2506.12729](https://doi.org/10.48550/arXiv.2506.12729)

Alush, Y., & Stone, N. C. 2025, ApJ, 993, 14, doi: [10.3847/1538-4357/adf217](https://doi.org/10.3847/1538-4357/adf217)

Angus, C. R., Baldassare, V. F., Mockler, B., et al. 2022, Nature Astronomy, 6, 1452, doi: [10.1038/s41550-022-01811-y](https://doi.org/10.1038/s41550-022-01811-y)

Bellm, E. C., Kulkarni, S. R., Graham, M. J., et al. 2019, PASP, 131, 018002, doi: [10.1088/1538-3873/aaecbe](https://doi.org/10.1088/1538-3873/aaecbe)

Cendes, Y., Berger, E., Alexander, K. D., et al. 2022, ApJ, 938, 28, doi: [10.3847/1538-4357/ac88d0](https://doi.org/10.3847/1538-4357/ac88d0)

—. 2024, ApJ, 971, 185, doi: [10.3847/1538-4357/ad5541](https://doi.org/10.3847/1538-4357/ad5541)

Charalampopoulos, P., Kotak, R., Wevers, T., et al. 2024, A&A, 689, A350, doi: [10.1051/0004-6361/202449296](https://doi.org/10.1051/0004-6361/202449296)

Faris, S., Arcavi, I., Makrygianni, L., et al. 2024, ApJ, 969, 104, doi: [10.3847/1538-4357/ad4a72](https://doi.org/10.3847/1538-4357/ad4a72)

Franz, N., Alexander, K. D., Gomez, S., et al. 2025, arXiv e-prints, arXiv:2509.05405, doi: [10.48550/arXiv.2509.05405](https://doi.org/10.48550/arXiv.2509.05405)

Gezari, S. 2021, ARA&A, 59, 21, doi: [10.1146/annurev-astro-111720-030029](https://doi.org/10.1146/annurev-astro-111720-030029)

Golay, W. W., Berger, E., Cendes, Y., et al. 2025, arXiv e-prints, arXiv:2508.16756, doi: [10.48550/arXiv.2508.16756](https://doi.org/10.48550/arXiv.2508.16756)

Goodwin, A. J., Burn, M., Anderson, G. E., et al. 2025, ApJS, 278, 36, doi: [10.3847/1538-4365/adbe80](https://doi.org/10.3847/1538-4365/adbe80)

Gris, P., Regnault, N., Awan, H., et al. 2023, ApJS, 264, 22, doi: [10.3847/1538-4365/ac9e58](https://doi.org/10.3847/1538-4365/ac9e58)

Guo, C., & Qiao, E. 2025, arXiv e-prints, arXiv:2509.16544, doi: [10.48550/arXiv.2509.16544](https://doi.org/10.48550/arXiv.2509.16544)

Guolo, M., Mummery, A., van Velzen, S., et al. 2025, arXiv e-prints, arXiv:2510.26774, doi: [10.48550/arXiv.2510.26774](https://doi.org/10.48550/arXiv.2510.26774)

Hammerstein, E., van Velzen, S., Gezari, S., et al. 2023, ApJ, 942, 9, doi: [10.3847/1538-4357/aca283](https://doi.org/10.3847/1538-4357/aca283)

Hills, J. G. 1975, Nature, 254, 295, doi: [10.1038/254295a0](https://doi.org/10.1038/254295a0)

Hinkle, J. T., Holoien, T. W.-S., Auchettl, K., et al. 2021, MNRAS, 500, 1673, doi: [10.1093/mnras/staa3170](https://doi.org/10.1093/mnras/staa3170)

Hinkle, J. T., Auchettl, K., Hoogendam, W. B., et al. 2024, arXiv e-prints, arXiv:2412.15326, doi: [10.48550/arXiv.2412.15326](https://doi.org/10.48550/arXiv.2412.15326)

Horesh, A., Cenko, S. B., & Arcavi, I. 2021, Nature Astronomy, 5, 491, doi: [10.1038/s41550-021-01300-8](https://doi.org/10.1038/s41550-021-01300-8)

Huang, X., Davis, S. W., & Jiang, Y.-f. 2024, ApJ, 974, 165, doi: [10.3847/1538-4357/ad6c39](https://doi.org/10.3847/1538-4357/ad6c39)

Huang, X., Meza, M. R., Yun, S. B., et al. 2025, arXiv e-prints, arXiv:2512.12985. <https://arxiv.org/abs/2512.12985>

Ivezić, Ž., Kahn, S. M., Tyson, J. A., et al. 2019, ApJ, 873, 111, doi: [10.3847/1538-4357/ab042c](https://doi.org/10.3847/1538-4357/ab042c)

Jiang, Y.-F., & Dai, L. 2024, arXiv e-prints, arXiv:2408.16856, doi: [10.48550/arXiv.2408.16856](https://doi.org/10.48550/arXiv.2408.16856)

Jiang, Y.-F., Stone, J. M., & Davis, S. W. 2019, ApJ, 880, 67, doi: [10.3847/1538-4357/ab29ff](https://doi.org/10.3847/1538-4357/ab29ff)

Law, N. M., Corbett, H., Galliher, N. W., et al. 2022, PASP, 134, 035003, doi: [10.1088/1538-3873/ac4811](https://doi.org/10.1088/1538-3873/ac4811)

Lin, Z., Jiang, N., Wang, T., et al. 2024, ApJL, 971, L26, doi: [10.3847/2041-8213/ad638e](https://doi.org/10.3847/2041-8213/ad638e)

Liu, X.-L., Dou, L.-M., Chen, J.-H., & Shen, R.-F. 2022, ApJ, 925, 67, doi: [10.3847/1538-4357/ac33a9](https://doi.org/10.3847/1538-4357/ac33a9)

Lu, W. 2022, in Handbook of X-ray and Gamma-ray Astrophysics, ed. C. Bambi & A. Sanganello (Springer), 3, doi: [10.1007/978-981-16-4544-0\\_127-1](https://doi.org/10.1007/978-981-16-4544-0_127-1)

Makrygianni, L., Arcavi, I., Newsome, M., et al. 2025, ApJL, 987, L20, doi: [10.3847/2041-8213/ade155](https://doi.org/10.3847/2041-8213/ade155)

Matsumoto, T., & Piran, T. 2021, MNRAS, 502, 3385, doi: [10.1093/mnras/stab240](https://doi.org/10.1093/mnras/stab240)

Mockler, B., Hammerstein, E., Coughlin, E. R., & Nicholl, M. 2025, arXiv e-prints, arXiv:2511.14911. <https://arxiv.org/abs/2511.14911>

Mummery, A. 2026, arXiv e-prints, arXiv:2601.14483, doi: [10.48550/arXiv.2601.14483](https://doi.org/10.48550/arXiv.2601.14483)

Mummery, A., & van Velzen, S. 2025, MNRAS, 541, 429, doi: [10.1093/mnras/staf938](https://doi.org/10.1093/mnras/staf938)

Mummery, A., van Velzen, S., Nathan, E., et al. 2024, MNRAS, 527, 2452, doi: [10.1093/mnras/stad3001](https://doi.org/10.1093/mnras/stad3001)

Nicholl, M., Wevers, T., Oates, S. R., et al. 2020, MNRAS, 499, 482, doi: [10.1093/mnras/staa2824](https://doi.org/10.1093/mnras/staa2824)

Onori, F., Nicholl, M., Ramsden, P., et al. 2025, MNRAS, 540, 498, doi: [10.1093/mnras/staf746](https://doi.org/10.1093/mnras/staf746)

Pasham, D. R., Zajaček, M., Nixon, C. J., et al. 2024, Nature, 630, 325, doi: [10.1038/s41586-024-07433-w](https://doi.org/10.1038/s41586-024-07433-w)

Phinney, E. S. 1989, in IAU Symposium, Vol. 136, The Center of the Galaxy, ed. M. Morris, 543

Piro, A. L., & Lu, W. 2020, ApJ, 894, 2, doi: [10.3847/1538-4357/ab83f6](https://doi.org/10.3847/1538-4357/ab83f6)

Piro, A. L., & Mockler, B. 2025, ApJ, 985, 77, doi: [10.3847/1538-4357/adc729](https://doi.org/10.3847/1538-4357/adc729)

Price, D. J., Liptai, D., Mandel, I., et al. 2024, ApJL, 971, L46, doi: [10.3847/2041-8213/ad6862](https://doi.org/10.3847/2041-8213/ad6862)

Rees, M. J. 1988, Nature, 333, 523, doi: [10.1038/333523a0](https://doi.org/10.1038/333523a0)

Ryu, T., Krolik, J., Piran, T., Noble, S. C., & Avara, M. 2023, ApJ, 957, 12, doi: [10.3847/1538-4357/acf5de](https://doi.org/10.3847/1538-4357/acf5de)

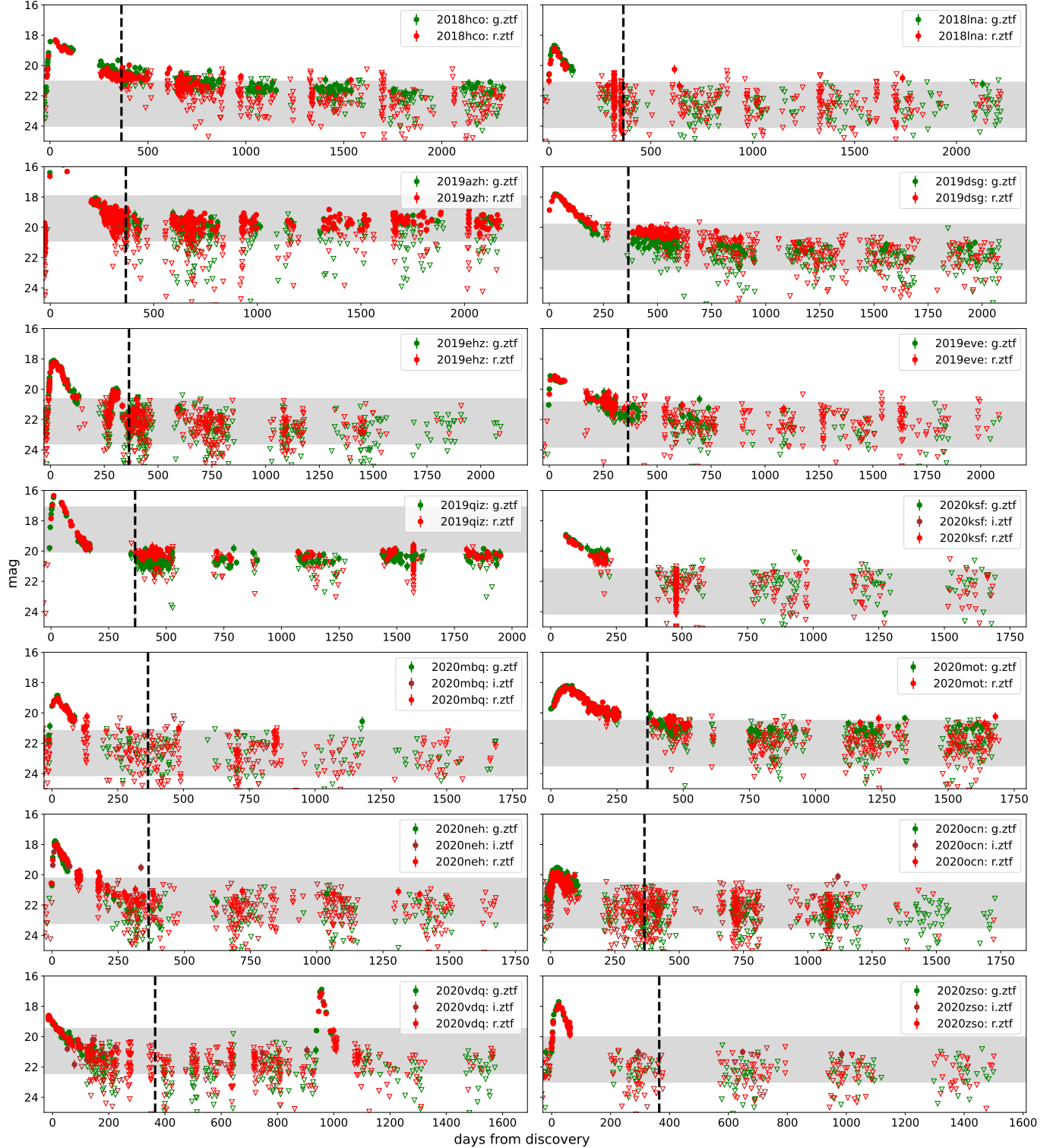


**Figure 7.** Host-corrected ZTF light curves of 28 TDEs selected from OTTER. Dashed lines show 1 year from discovery, and we search for flares beyond this epoch. Filled circles denote detections ( $S/N > 3$ ), and open triangles denote upper limits ( $S/N < 3$ ). Grey shaded regions show the flare magnitude for an expected absolute magnitude of  $(-14) - (-17)$  mag (see Section 3).

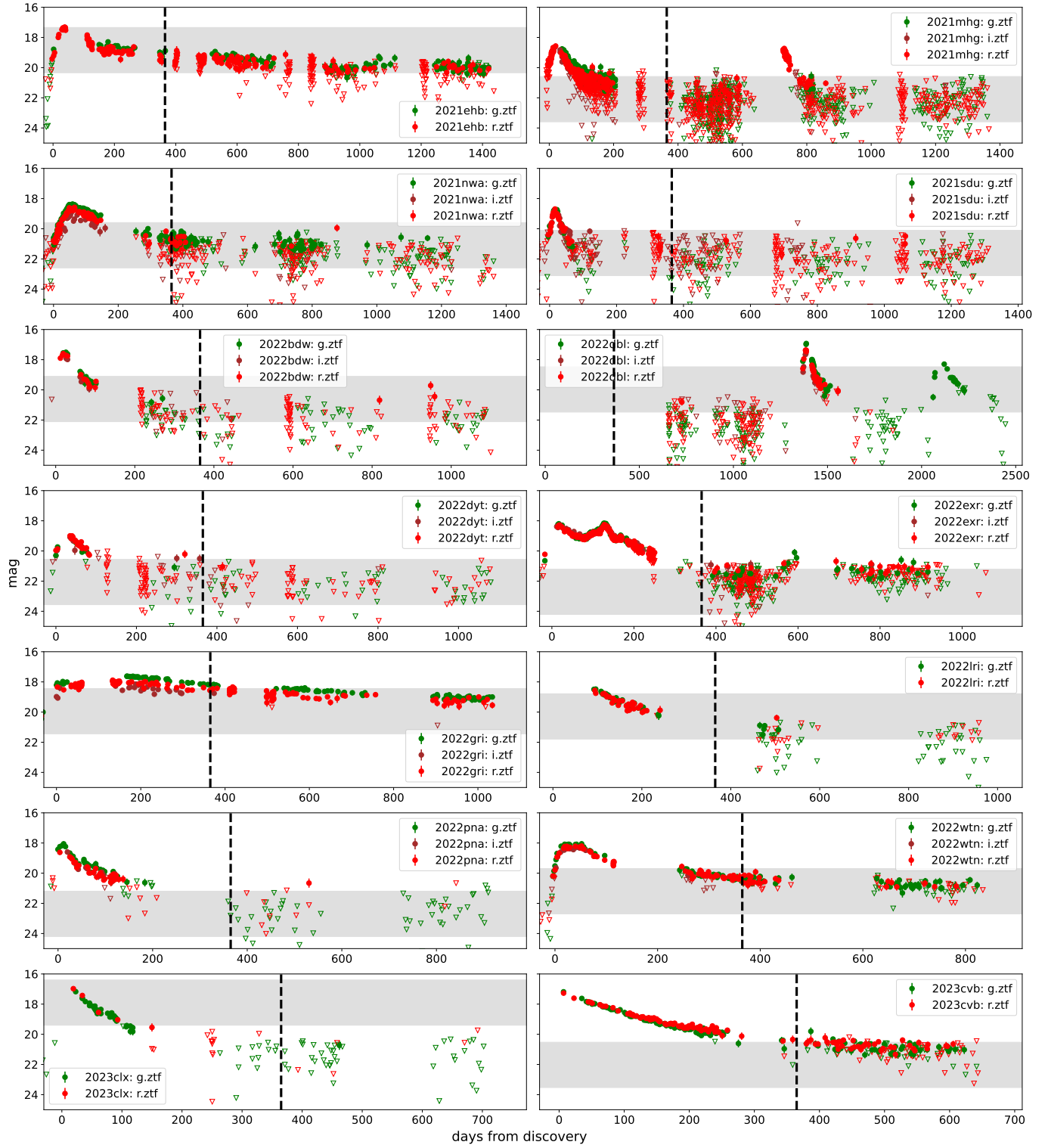


Figure 7. (Continued)

Sato, Y., Bhattacharya, M., Carpio, J., Capili, J., & Murase, K. 2025, arXiv e-prints, arXiv:2512.23252, doi: [10.48550/arXiv.2512.23252](https://doi.org/10.48550/arXiv.2512.23252)

Saxton, R., Komossa, S., Auchettl, K., & Jonker, P. G. 2021, Correction to: X-Ray Properties of TDEs, *Space Science Reviews*, Volume 217, Issue 1, article id.18, doi: [10.1007/s11214-020-00759-7](https://doi.org/10.1007/s11214-020-00759-7)

Sfaradi, I., Beniamini, P., Horesh, A., et al. 2024, MNRAS, 527, 7672, doi: [10.1093/mnras/stad3717](https://doi.org/10.1093/mnras/stad3717)

Shakura, N. I., & Sunyaev, R. A. 1973, A&A, 24, 337

Shvartzvald, Y., Waxman, E., Gal-Yam, A., et al. 2024, ApJ, 964, 74, doi: [10.3847/1538-4357/ad2704](https://doi.org/10.3847/1538-4357/ad2704)

Somalwar, J. J., Ravi, V., Yao, Y., et al. 2025a, ApJ, 985, 175, doi: [10.3847/1538-4357/adcc19](https://doi.org/10.3847/1538-4357/adcc19)

Somalwar, J. J., Ravi, V., Dong, D. Z., et al. 2025b, ApJ, 982, 163, doi: [10.3847/1538-4357/adba4f](https://doi.org/10.3847/1538-4357/adba4f)

Steinberg, E., & Stone, N. C. 2024, Nature, 625, 463, doi: [10.1038/s41586-023-06875-y](https://doi.org/10.1038/s41586-023-06875-y)

van Velzen, S., Stone, N. C., Metzger, B. D., et al. 2019, ApJ, 878, 82, doi: [10.3847/1538-4357/ab1844](https://doi.org/10.3847/1538-4357/ab1844)

van Velzen, S., Gezari, S., Hammerstein, E., et al. 2021, ApJ, 908, 4, doi: [10.3847/1538-4357/abc258](https://doi.org/10.3847/1538-4357/abc258)

Wevers, T., Guolo, M., Pasham, D. R., et al. 2024, ApJ, 963, 75, doi: [10.3847/1538-4357/ad1878](https://doi.org/10.3847/1538-4357/ad1878)

Wevers, T., Nicholl, M., Guolo, M., et al. 2022, A&A, 666, A6, doi: [10.1051/0004-6361/202142616](https://doi.org/10.1051/0004-6361/202142616)

Wu, S. C., Tsuna, D., Mockler, B., & Piro, A. L. 2025, arXiv e-prints, arXiv:2511.14008, doi: [10.48550/arXiv.2511.14008](https://doi.org/10.48550/arXiv.2511.14008)

Yao, Y., Lu, W., Guolo, M., et al. 2022, ApJ, 937, 8, doi: [10.3847/1538-4357/ac898a](https://doi.org/10.3847/1538-4357/ac898a)

Yao, Y., Ravi, V., Gezari, S., et al. 2023, ApJL, 955, L6, doi: [10.3847/2041-8213/acf216](https://doi.org/10.3847/2041-8213/acf216)

Yao, Y., Guolo, M., Tombesi, F., et al. 2024, ApJ, 976, 34, doi: [10.3847/1538-4357/ad7d93](https://doi.org/10.3847/1538-4357/ad7d93)

Yoshioka, S., Mineshige, S., Ohsuga, K., Kawashima, T., & Kitaki, T. 2024, PASJ, 76, 1015, doi: [10.1093/pasj/psae067](https://doi.org/10.1093/pasj/psae067)

Zhang, L., Stone, J. M., White, C. J., et al. 2025, arXiv e-prints, arXiv:2509.10638, doi: [10.48550/arXiv.2509.10638](https://doi.org/10.48550/arXiv.2509.10638)

Zhu, J., Jiang, N., Wang, Y., et al. 2025, ApJL, 994, L16, doi: [10.3847/2041-8213/ae19ea](https://doi.org/10.3847/2041-8213/ae19ea)